Humidity Measurements in Carbon Dioxide with Sensirion SHT85 Humidity Sensors under simulated Martian atmospheric conditions

5 Andreas Lorek[1], Stephen Garland[1]

[1]German Aerospace Center (DLR), Berlin, 12489, Germany

Correspondence to: Andreas Lorek (andreas.lorek@dlr.de)

Abstract. Humidity sensors that function under extreme conditions are needed in experimental chambers in which the atmospheric conditions near the surface of Mars are simulated, as well as for in-situ measurements of humidity on the surface 10 of Mars. Experimental setups with such sensors have already been constructed at the German Aerospace Center (DLR) and published. However, the SHT75 sensors from Sensirion used at that time are no longer in production and have been replaced by a new generation of sensors: SHT85. The SHT85 sensors are more precise than their predecessors, have a new sensor chip, and feature a PTFE membrane over the humidity-sensitive layer to protect the sensor from dust and liquids. The data interface to the I2C bus has also changed. Due to these significant changes, it was necessary to verify the sensor's capabilities under 15 extreme conditions. For this purpose, the sensors were tested under the same conditions and in parallel to the calibration of the MEDA HS sensor from the Finnish Meteorological Institute (FMI), onboard NASA's Mars 2020 rover. The results show that the SHT85 is, as its predecessor SHT75, suitable for measurements under Martian atmospheric conditions when the relative humidity is in the range >5%.

1 Introduction

20 The SHT85 sensors from Sensirion AG are polymer-based capacitive humidity sensors. This kind of sensor can work under extreme conditions, leading to applications for in-situ humidity measurements on Mars (Gómez-Elvira et al., 2012; Witte et al., 2022; Zent et al., 2016) and in Mars simulation chambers (Jensen et al., 2008). An overview of the performance of a capacitive polymer sensor (MEDA HS) under Martian conditions is published in (Hieta et al., 2022). In the Planetary Analogue Simulation Laboratory (PASLAB) at the German Aerospace Institute (DLR) such sensors are used in an experiment chamber 25 for Mars exposure simulations (Lorek and Majewski, 2018). Up until now SHT75 sensors from Sensirion AG were used inside the chamber, however due to termination of the production of the SHT75, and the good experience with this sensor (Lorek, 2014; Lorek and Majewski, 2018), the SHT85 was considered as a replacement. The SHT85 have significant changes

compared to SHT75 (Anon, 2018) (Fig. 1) such as a PTFE membrane, new humidity sensitive chip, higher precision and a new data interface.

30
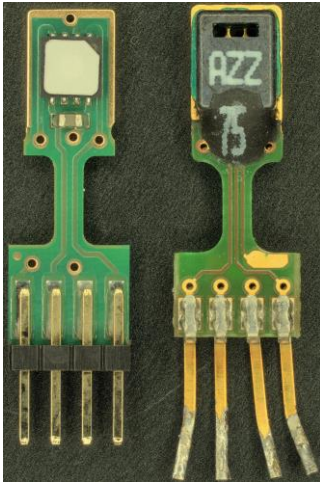
Figure 1: SHT85 (left) and SHT75 (right) (Lorek et al., 2024)

With the SHT75 extensive experiments in air and CO_2 were made in the temperature range -70° C to 10° C, pressure range
35 10 hPa to 1000 hPa and relative humidity ($U_{w,i}$ - w, i respect to water, ice) range from around 5% to 95% (Lorek, 2014; Lorek and Majewski, 2018)).

The Finnish Meteorological Institute (FMI) successful calibrated its MEDA HS, REMS-H and METEO-H sensors (Hieta et al., 2022, 2024) at PASLAB in 2020/21. In parallel to this calibration campaign, and under the same conditions, six SHT85 sensors were tested to evaluate their performance under extreme conditions compared to the SHT75.

40 **2 Experimental Procedure**

Experiments were conducted at the humidity sensor calibration facility at PASLAB, DLR Berlin. An overview of the experimental setup is shown in Figure 2. Generally, CO_2 was used for the experiments, apart from a few where air was used. In both cases, dry gas was mixed with precisely humidified gas using mass flow controllers (MFCs) in the gas mixing system. The resulting gas, with a defined water content, flowed via stainless steel tubing through two MFC outputs to the measurement
45 cells housing the sensors and over a third to the reference humidity measurement: a dew point mirror (MBW 373LX). The measurement cells were mounted in a temperature test chamber (Weiss KWP 240). The measurement cell was made from stainless steel and comprised two measurement chambers (see (Lorek, 2014; Lorek and Majewski, 2018) for more details). A Pfeiffer Vacuum CMR 361 pressure sensor was used to measure pressure inside the measurement cell. After passing through

the chambers the gas flow was directed to a vacuum pump (Vacuubrand MV10 Vario) which was used to set the pressure in
50   the chambers.
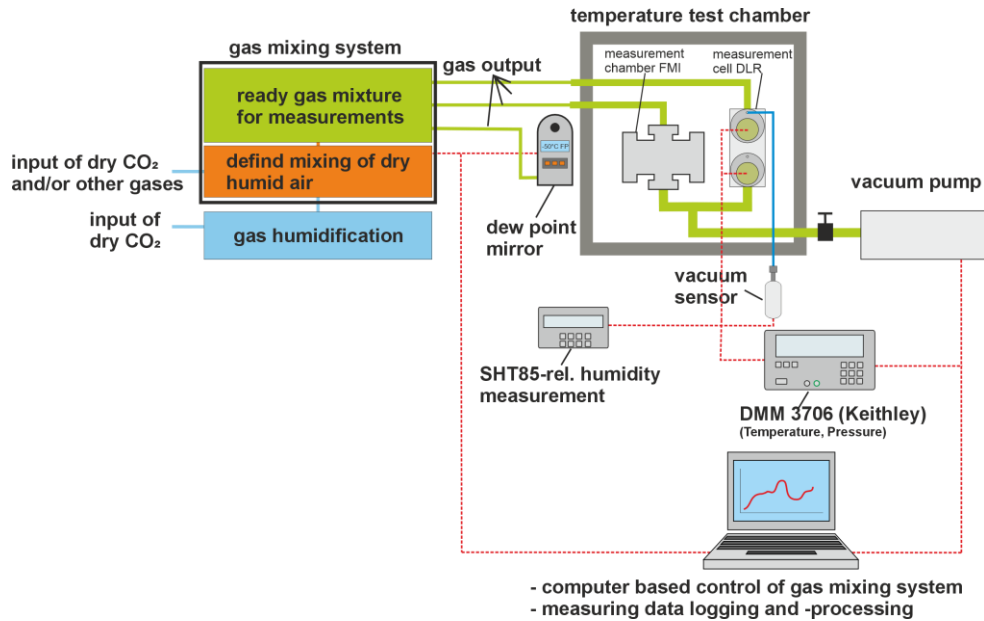
Figure 2: This figure of the experiment setup based on Figure 9a from (Hieta et al., 2022).

The sensor measurement head is shown in Figure 3. Three SHT85 and four Pt100 (POK1.232.6W.Y.007 IST AG) were placed
55   in each of the measuring chambers comprising the measuring cell. As in the previous experiments (Lorek, 2014), a Pt100 was
glued onto the back of each SHT85 sensor since the measuring limit for the SHT85 temperature sensor is -40° C and
temperatures down to -70° C were set during experiments. The fourth Pt100 was centered between the SHT/Pt100 combined
sensors.

60   **Figure 3: sensor configuration in chamber 1**

Table 1 shows the naming convention for each sensor used in this paper.

nomenclature	SHT	Pt100 on SHT85	Pt100 in center
measuring chamber 1	Z1SHT-1 Z1SHT-2 Z1SHT-3	Z1PtS1 Z1PtS2 Z1PtS3	Z1Pt1
measuring chamber 2	Z2SHT-4 Z2SHT-5 Z2SHT-6	Z2PtS4 Z2PtS5 Z2PtS6	Z2Pt1

65 **Table 1: Nomenclature of each SHT85 and Pt100 sensor.**

The ranges of the relative humidity for every temperature–pressure combination used during the experiments are listed in Table 2. Test runs began at the driest humidity points and increased in steps of 5, 10 to 20 % $U_{i,w}$. At each step the humidity was kept stable over several hours. After reaching the highest humidity, the humidity was lowered again in the same way

70 (Figure 7). The main procedure of the experiment is described in (Hieta et al., 2022; Lorek, 2014; Lorek and Majewski, 2018).

T	p in air	p in CO_2		
	1000 hPa	**6 hPa**	**8 hPa**	**10 hPa**
22° C	47 5			
10° C	93 9			
0° C	93 5			
-30° C			21 (28) 4 (5)	
-40° C		40 (60) 3 (5)	57 (84) 3 (5)	66 (97) 3 (5)
-50° C		57 (93) 3 (4)	58 (97) 2 (3)	48 (78) 3 (4)
-60° C		51 (92) 3 (5)	51 (91) 2 (4)	51 (92) 2 (4)
-70° C		49 (97) 2 (5)	42 (84) 2 (4)	47 (92) 2 (4)

Table 2: Range of the relative humidity in air and CO_2 under investigation for the different temperature and pressure conditions. Relative humidity is calculated with respect to water U_w or ice U_i (marked by brackets).

75

The measurement at -30 °C and 8 hPa was for orientation only. Due to the construction of the gas mixing and humidification system the highest reachable humidity is approximately 10 to 11° C dew point at 1 atm pressure. This leads to a U_i of

approximately 30 % of the maximum at -30 °C and 8 hPa, which was deemed insufficient for a complete fit over the full relative humidity range. For this reason, the measurements were not repeated at 6 and 10 hPa.

80 ## 3. Results

The relative humidity is given as U, with U_w for temperatures > 0° C and U_i for temperatures ≤ 0° C. The calculation is based on Eq. (1-3) (Anon, 2012) as used in (Lorek, 2014). In addition, the parameters are the water vapor partial pressure, e (hPa), the saturation vapor pressure under saturation conditions above a planar water or ice surface, e_w (hPa) and e_i (hPa) respectively, at total pressure p (hPa), temperature T (K) and T_1 = 273.16 K (triple point temperature of water).

85

$$U_{w,i} = \left(\frac{e}{e_{w,i}}\right)_{p,T} \cdot 100\% \tag{1}$$

Equation (2) is valid in the temperature range from 0 to 100° C:

90
$$\log_{10} e_w = 10.79574 \cdot \left(1 - \frac{T_1}{T}\right) - 5.028 \cdot \log_{10}\left(\frac{T_1}{T}\right) + 1.50475 \cdot 10^{-4} \cdot \left[1 - 10^{-8.2969 \cdot \left\{\frac{T}{T_1}\right\}}\right] + 0.42873 \cdot 10^{-3} \cdot$$
$$\left[10^{+4.76955 \cdot \left\{1 - \frac{T}{T_1}\right\}} - 1\right] + 0.78614, \tag{2}$$

and Eq. (3) is valid in the temperature range from -100° C to 0° C:

95
$$\log_{10} e_i = -9.09685 \cdot \left(\frac{T_1}{T} - 1\right) - 3.56654 \cdot \log_{10}\left(\frac{T_1}{T}\right) + 0.87682 \cdot \left(1 - \frac{T_1}{T}\right) + 0.78614. \tag{3}$$

3.1. Comparison with manufacturer's data of the SHT85 in air

Figure 4 shows the relative humidity of the SHT85 versus the derived relative humidity of the reference system ($U_{i,w\ (ref)}$), which consists of the dew point mirror, the pressure sensor and the free standing Pt100. The relative humidity values of the SHT85 ($U_{w\ SHT85}$) are calculated from the Eq. (4).

100
$$U_{w\ SHT85} = 100\% \cdot \frac{S_{RH}}{2^{16}-1}, \tag{4}$$

where, S_{RH} is the raw digital sensor output of the SHT85.

105 The error bar for the X-axis is +/-1.5% $U_{w\,(SHT85)}$ (Anon, 2021). For the Y-axis, the estimated error bar is +/-5% of the measurement value $U_{w\,(ref)}$ based on a 2σ error estimate for the CMR 361 pressure sensor of 0.2 % of the measurement value, 0.3° C of the Pt100 and 0.1° C of the MBW LX373 Dew point mirror.
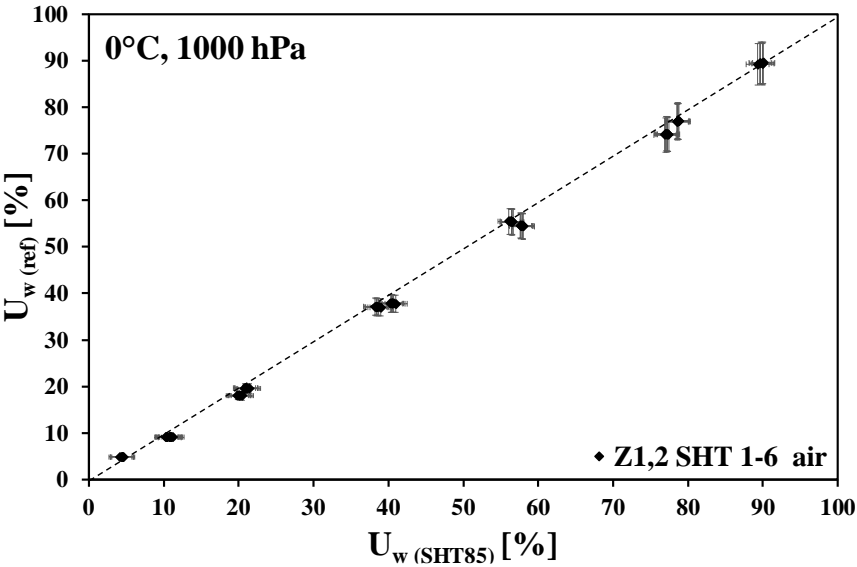
Figure 4: The relative humidity values from the reference system (air, 0° C, 1000 hPa) as a function of the humidity values of all six
110 **SHT85 calculated using Eq. (4).**

All U_w values from the SHT85 lie, to within the error bars, on the dotted line, which represents a 1:1 agreement of $U_{w\,(SHT85)}$ and $U_{w\,(ref)}$. This indicates that the adhesion of a Pt100 temperature sensor to the back of the SHT85 does not significantly affect their performance.

115 **3.2. Comparison of the SHT75 and SHT85 data in air and CO$_2$**

Comparing Fig. 5a (SHT75 data) with Fig. 5b (SHT85 data), it can be seen that both sensors behave similarly. Both sensors show a strong cross-sensitivity to CO$_2$. Whereby the SHT75 in Figure 5a has a more non-linear calibration function in CO$_2$ compared to the SHT85.
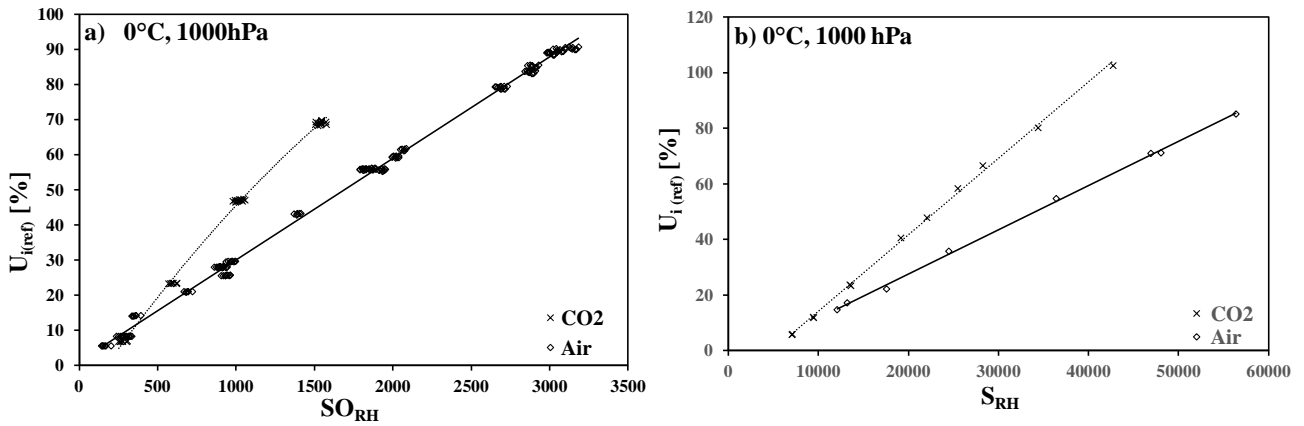
120 Figure 5: Reference humidity as a function of a) SHT75 raw output values (SORH) (Lorek and Majewski, 2018) and

b) SHT85 raw output values (SRH) at 0° C, and atmospheric pressure with air and CO₂.

3.3. Comparison of the SHT85 temperature measurement with independent Pt100 measurements

Figure 6 shows the temperature measurements from the SHT85 along with the independent measurement from Pt100 sensors at different temperatures and pressures. The pressures (6hPa, 8hPa, 10hPa and 1000hPa) were held stable whilst temperature

125 was varied stepwise within an experimental run. Figure 6a shows the reaction of the six adhered Pt100s (Z1PtS1 – Z2PtS6) and the two free-floating Pt100s (Z1Pt1 and Z2Pt1) (see Table 1 and Fig. 3). The free-floating Z1Pt1 and Z2Pt1 sensors measure a temperature approximately 0.15° C lower than the adhered Pt100. This lies within the 2σ error of 0.3° C, similar to the previous observations (Lorek, 2014). The cause for this is probably self-heating of the SHT85. The internal SHT85 temperatures displayed in Fig. 6b show a comparable temperature under the same conditions as Fig. 6a (0° C, 1000 hPa, air).

130 A similar behavior (Fig. 6c compared to Fig. 6d) is observable at -40° C, 6 to 10 hPa in CO₂. At -70° C (Fig. 6e) only the Pt100 are displayed because the lowest measurable temperature for the SHT85 is -45° C. In all cases the difference between Z1Pt1 and Z2Pt1 and the adhered Pt100 Z1PtS1 – Z2PtS6 is approximately 0.15° C, which is within the nominal error range quoted by the manufacturers for these sensors.
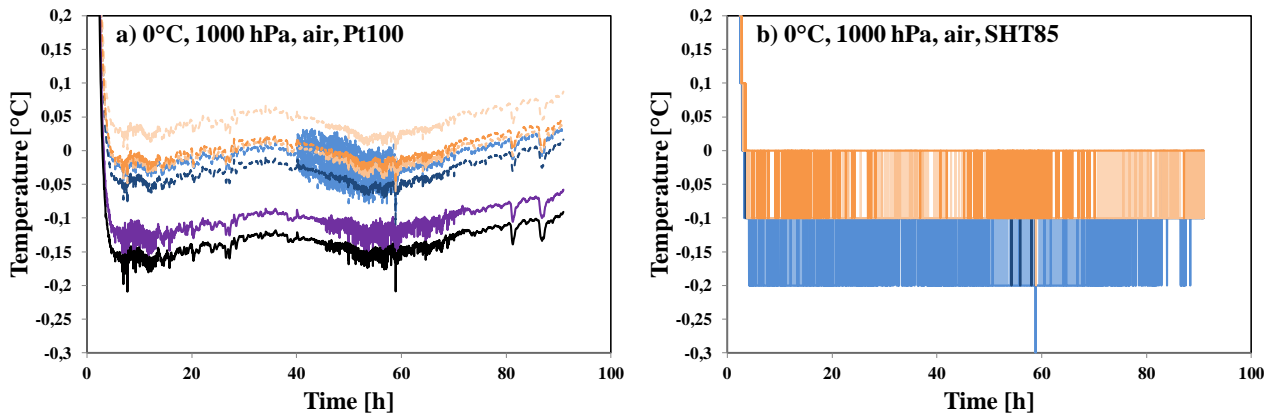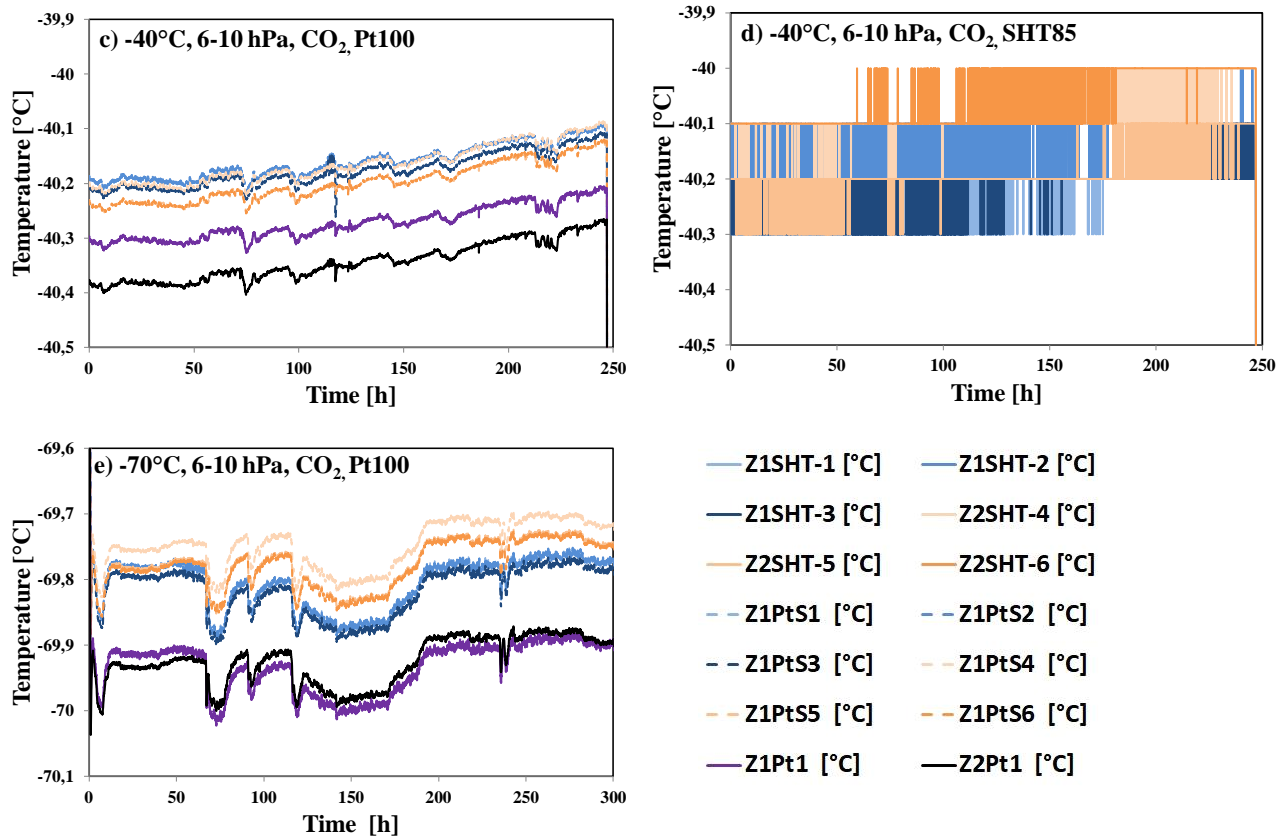
Figure 6. (a, c and e): Temperature curves of the adhered Pt100 (Z1PtS1 – Z1PtS6), the free-floating Pt100s (Z1Pt1, Z2Pt1). (b and d): the temperature readout from the SHT85 at different chamber temperatures.

3.4. Comparison of the SHT85 humidity measurement in CO_2 as a function of temperature

The experiments were performed with CO_2 in the Martian-relevant pressure range of 6 to 10 hPa. Separate experimental runs were performed for the pressures 6 hPa, 8 hPa and 10 hPa. For each pressure the temperatures -40° C, -50° C, -60° C and -70° C (Table 2) were set. For the temperature -30° C measurements were made only at 8 hPa. Figure 7 shows an example for a typical experimental run for the six SHT85. In this case the conditions were 8 hPa, -40° C, CO_2.

145
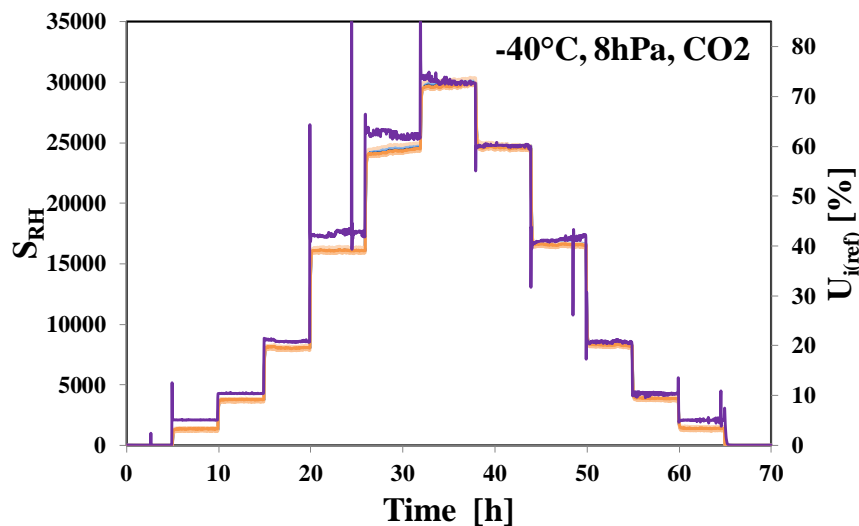
Figure 7: A typical experimental run (conditions CO₂, -40° C. 8hPa), lila line U_i (ref) -values, other lines represent the S_RH -values of the six SHT85.

![Four scatter plots a) -30°C, b) -40°C, c) -50°C, d) -60°C showing U_i(ref) [%] versus S_RH]

150
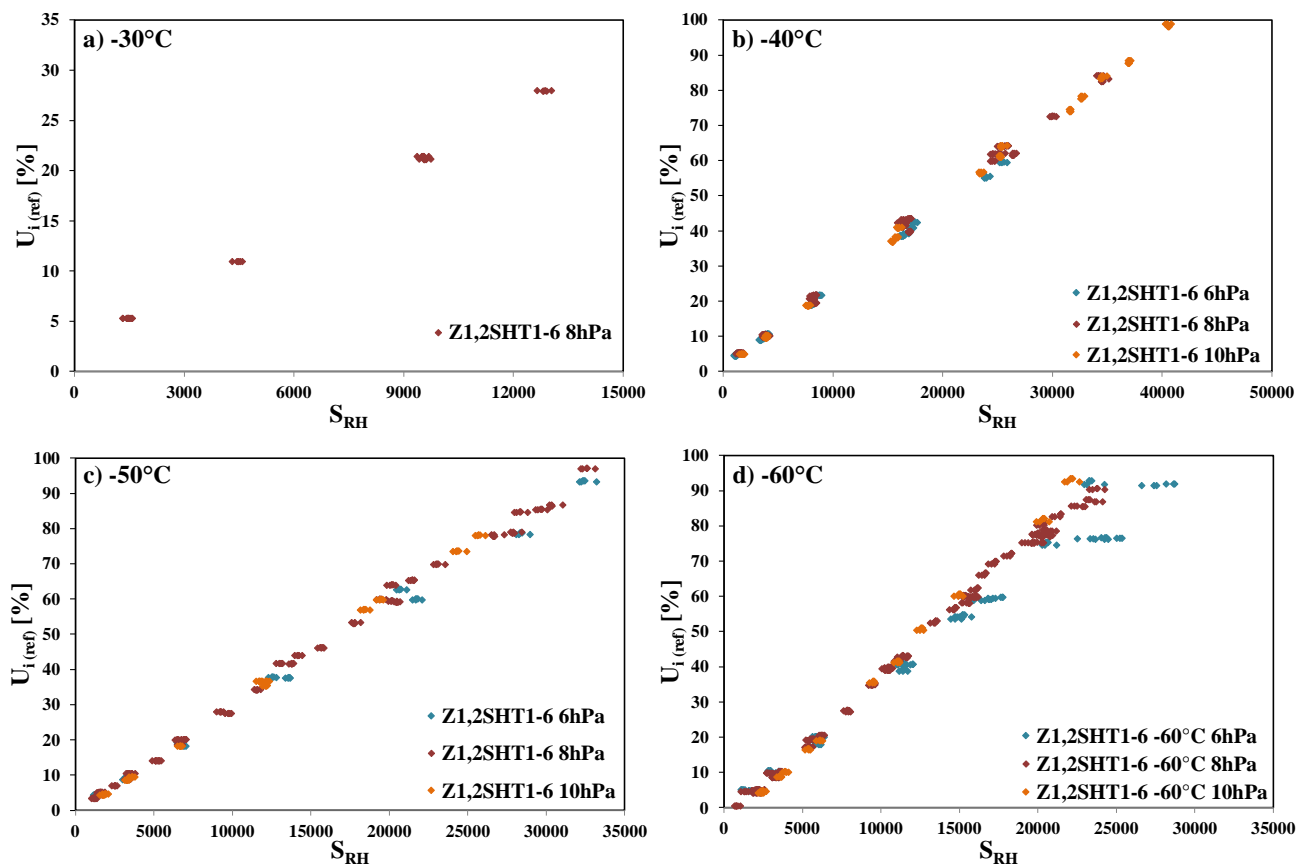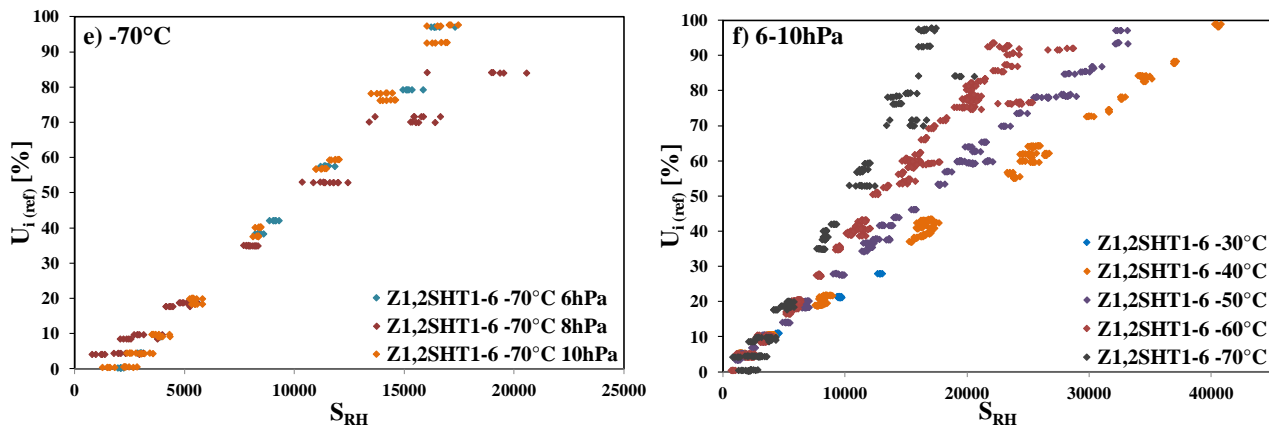
Figure 8: a-e) show the independently measured relative humidity, $U_{i(ref)}$, as a function of the sensor raw output, S_{RH}, at constant temperatures for pressures 6, 8, 10 hPa. In f) all the data is displayed together for temperatures in the range -30° C to -70° C.

Figure 8 shows that the SHT85 sensitivity decreases with temperature, resulting in lower raw output values, S_{RH}, for a given
155   relative humidity. In addition, the scatter of the measured values increases with decreasing temperature. In Fig. 8d there is a
spread in the data from the six SHT85 sensors during the 6 hPa run, which is not seen in the data at 8 and 10 hPa. A similar
behavior can be seen in Fig. 8e at 8 hPa, where five of six SHT85 are not in line with the other runs at 6 hPa and 10 hPa. The
reason for this different behavior is not clear. The experimental runs exhibiting different behavior took place at the beginning
of new temperature steps at lower temperatures, below -50 °C, as well as at the standard of the new measurement campaigns
160   at different pressures. Although the cause of the deviant behavior is unclear, it is likely to be due to a time lag in the adaptation
of the polymer to new temperature or pressure conditions (desorption of molecules or a phase change from water to ice) or a
time lag in the adaption of the electronics inside the SHT85. A significant difference between the investigated pressures 6, 8,
10 hPa is not observable, allowing the data to be analyzed together (Fig. 8f, 9).

Figure 9 shows the same values as in Fig. 8f with linear regression fits for each temperature. The data showing unexpected
165   behavior, as discussed above, was excluded from this figure. From the figure the decrease in sensitivity of the sensors with
decreasing temperature can clearly be seen. This results in a reduction in resolution with decreasing temperatures which leads
to larger uncertainties in the relative humidity. Indeed, the usable temperature range for the SHT85 under Martian-like
atmospheric conditions is unlikely to extend much below -80° C due to decreasing humidity resolution and the associated error
on the humidity. With the experimental setup used it was not possible to quantify this limit since temperatures below -70° C
170   are not possible.
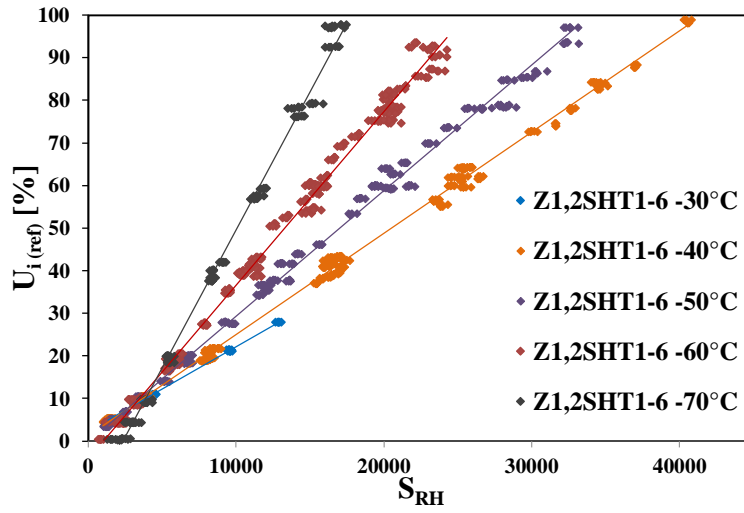
Figure 9: The data from Figure 8f, excluding outliers, with linear regression fits for each temperature.

temperature	fit equation
-30° C	$U_{i(ref)} = 0.0020 \cdot S_{1RH} + 2.2809$
-40° C	$U_{i(ref)} = 0.0024 \cdot S_{1RH} + 1.2008$
-50° C	$U_{i(ref)} = 0.0029 \cdot S_{1RH} - 0.0672$
-60° C	$U_{i(ref)} = 0.0041 \cdot S_{1RH} - 4.1136$
-70° C	$U_{i(ref)} = 0.0065 \cdot S_{1RH} - 15.115$

175 **Table 3: linear fit equations of the data from Figure 9 for each temperature in the pressure range 6 to 10 hPa**

The equations in Table 3 are written in the following form:

180 $\qquad U_{i(ref)} = a_1 \cdot S_{1RH} + a_0.$ (5)

The dependence of the parameters a_0 and a_1 in relation to the temperature T_C (° C), (-30 to -70° C) at pressures of 6 to 10 hPa is given by the Eq. (6) and (7):

185 $\qquad a_0 = 5.761 \cdot 10^{-4} \cdot T_C^3 + 7.001 \cdot 10^{-2} \cdot T_C^2 + 2.888 \cdot T_C + 41.5$ (6)

$\qquad a_1 = -9.369 \cdot 10^{-8} \cdot T_C^3 - 1.063 \cdot 10^{-5} \cdot T_C^2 - 4.361 \cdot 10^{-4} \cdot T_C - 4.045 \cdot 10^{-3}$ (7)

Figure 10 shows the fits of a_0 and a_1. Comparing the fits of a_0 and a_1 with those calculated for the SHT75 (Lorek and Majewski, 2018), a_0 has a different shape but a_1 is similar.

190
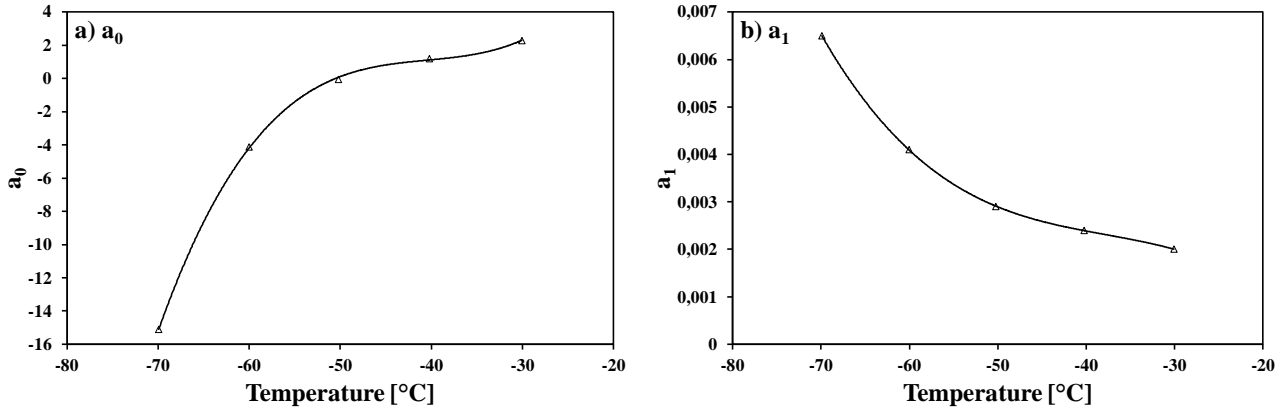
Figure 10: a) fit parameters a_0 and b) a_1 as a function of temperature.

With Eq. (8) the relative humidity (U_{calc}) can be determined using the temperature and S_{RH} values for the pressure range 6-10 hPa. This equation was obtained by inserting Eq. (6) and (7) into Eq. 5. A similar approach was uses in (Lorek, 2014; Lorek

195 and Majewski, 2018).

$U_{calc} = (-9.369 \cdot 10^{-8} \cdot T_C^3 - 1.063 \cdot 10^{-5} \cdot T_C^2 - 4.361 \cdot 10^{-4} \cdot T_C - 4.045 \cdot 10^{-3}) \cdot S_{RH} + 5.761 \cdot 10^{-4} \cdot T_C^3 + 7.001 \cdot 10^{-2} \cdot T_C^2 + 2.888 \cdot T_C + 41.5$ (8)

200 Figure 11 shows the results from Eq. (8) applied to the S_{RH} values in Fig. 9 and a comparison with the SHT75 data for 10 hPa based on Fig. 2d and Eq. (1, 2) and Table 3 from (Lorek and Majewski, 2018).
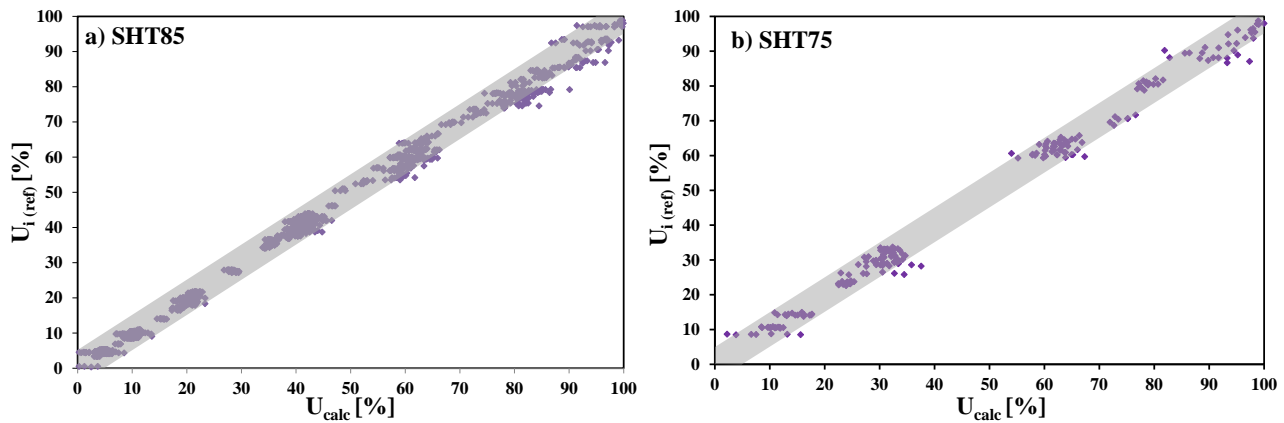
Figure 11: a) all calculated SHT85 values and b) all calculated SHT75 values replotted from (Lorek and Majewski, 2018) **in relation to the reference values; (gray area +/- 5 % U for orientation)**

205

With the SHT85 it is possible to measure under Martian like conditions, as was the case with the SHT75 data for 10 hPa (Lorek and Majewski, 2018). In addition, Fig. 11 shows that the SHT85 have a similar uncertainty in U_{calc} as the SHT75, with the caveat of a deviation from the expected behavior at -60° C and -70° C at specific pressures. This outlying data was excluded in Fig. 9 and the fit parameters for Eq. (8). A similar behavior was not observed during the experiments with SHT75 (Lorek, 210 2014; Lorek and Majewski, 2018). All six SHT85 survived the experiments under Martian conditions, for a total of 2150 hours, and delivered the same calibration curve at the end compared to the beginning of the experiments (Fig. 12).
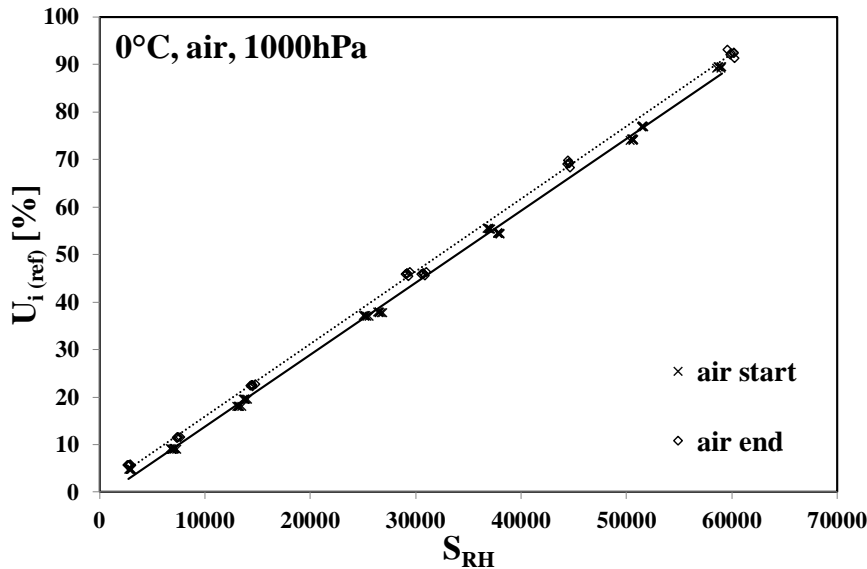
Figure 12: Measurement data in air, 0° C at the start (solid) and the end (dotted) of the experimental campaign.

4 Summary and conclusion

A measurement campaign was carried out for the SHT85, the new generation of humidity sensor from Sensirion, to test their measurement capability under Martian-like atmospheric conditions: CO_2 atmosphere, temperatures in the range -70 to -30° C, and pressures in the range 6-10 mbar. Reference measurements were made with a dew point mirror. The measurement campaign was carried out simultaneously to the calibration campaign of the MEDA HS humidity sensors on the Mars 2020 Perseverance Rover CITE using a parallel but distinct measurement chamber. The measurement campaign follows on from previous tests of the discontinued SHT75 sensor, deployed in the past in experiments under Martian atmospheric conditions at PASLAB, DLR Berlin.

Due to the lower temperature limit of -40° C for the inbuilt SHT85 temperature sensors, Pt100 sensors were adhered to the back of the SHT85 using a heat conducting ceramic glue. In addition, a free floating Pt100 was included in each measurement chamber. The free floating Pt100s measured temperatures of the order of 0.15° C lower than the Pt100s adhered to the SHT85, assumed to be due to the self-heating of the humidity sensors. This temperature discrepancy is, however, inside the nominal measurement error of the sensors.

As with the previously characterized SHT75, the SHT85 show a reduced sensitivity when measuring in CO_2, resulting in a reduced humidity resolution. A further reduction in sensitivity is observed with reducing temperature resulting in only around 30% of the dynamic range of the sensor being used at -70° C in CO_2. No strong pressure dependence was observed in the Martian pressure range 6-10 mbar. Linear fits were made to the measurements to obtain calibration functions for the SHT85 for each temperature. A temperature dependent calibration function was determined by fitting third order polynomials to the linear fit parameters as a function of temperature. The final result is an updated conversion function for the Sensirion SHT85 humidity sensors applicable in a CO_2 atmosphere in the pressure range 6-10 mbar and temperature range -70 to -30° C. The sensors can be deployed in this parameter space without being permanently affected, and return to normal operation in air after extended periods of use under Martian-like atmospheric conditions.

Competing interests: The authors declare that they have no conflict of interest.

References

Anon: Technical Regulations Basic Documents No. 2 Volume I – General Meteorological Standards and Recommended Practices, 2012.

Anon: Transitioning from SHT7x to SHT85, 2018.

Anon: Datasheet SHT85, 2021.

Gómez-Elvira, J., Armiens, C., Castañer, L., Domínguez, M., Genzer, M., Gómez, F., Haberle, R., Harri, A.-M., Jiménez, V., Kahanpää, H., Kowalski, L., Lepinette, A., Martín, J., Martínez-Frías, J., McEwan, I., Mora, L., Moreno, J., Navarro, S., de Pablo, M. A., Peinado, V., Peña, A., Polkko, J., Ramos, M., Renno, N. O., Ricart, J., Richardson, M., Rodríguez-Manfredi, J., Romeral, J., Sebastián, E., Serrano, J., de la Torre Juárez, M., Torres, J., Torrero, F., Urquí, R., Vázquez, L., Velasco, T., Verdasca, J., Zorzano, M.-P., and Martín-Torres, J.: REMS: The Environmental Sensor Suite for the Mars Science Laboratory Rover, Space Sci. Rev., 170, 583–640, https://doi.org/10.1007/s11214-012-9921-1, 2012.

Hieta, M., Genzer, M., Polkko, J., Jaakonaho, I., Tabandeh, S., Lorek, A., Garland, S., de Vera, J.-P., Fischer, E., Martínez, G. M., Harri, A.-M., Tamppari, L., Haukka, H., Meskanen, M., de la Torre Juárez, M., and Rodriguez Manfredi, J. A.: MEDA HS: Relative humidity sensor for the Mars 2020 Perseverance rover, Planet. Space Sci., 223, 105590, https://doi.org/10.1016/j.pss.2022.105590, 2022.

Hieta, M., Jaakonaho, I., Polkko, J., Lorek, A., Garland, S., De Vera, J.-P., Genzer, M., and Harri, A.-M.: Improving relative humidity measurements on Mars: new laboratory calibration measurements, Geosci. Instrum. Methods Data Syst., 13, 337–351, https://doi.org/10.5194/gi-13-337-2024, 2024.

Jensen, L. L., Merrison, J., Hansen, A. A., Mikkelsen, K. A., Kristoffersen, T., Nørnberg, P., Lomstein, B. A., and Finster, K.: A Facility for Long-Term Mars Simulation Experiments: The Mars Environmental Simulation Chamber (MESCH), Astrobiology, 8, 537–548, https://doi.org/10.1089/ast.2006.0092, 2008.

Lorek, A.: Humidity measurement with capacitive humidity sensors between −70°C and 25°C in low vacuum, J. Sens. Sens. Syst., 3, 177–185, https://doi.org/10.5194/jsss-3-177-2014, 2014.

Lorek, A. and Majewski, J.: Humidity Measurement in Carbon Dioxide with Capacitive Humidity Sensors at Low Temperature and Pressure, Sensors, 18, 2615, https://doi.org/10.3390/s18082615, 2018.

Lorek, A., Garland, S. P., Baqué, M., and Helbert, J.: THE PLANETARY ANALOG SIMULATION LABORATORY (PASLAB), 55th Lunar and Planetary Science Conference, The Woodlands, Texas, 2024.

Witte, L., Arnold, G., Bertram, J., Grott, M., Krämer, C., Lorek, A., and Wippermann, T.: A Concept for a Mars Boundary Layer Sounding Balloon: Science Case, Technical Concept and Deployment Risk Analysis, Aerospace, 9, https://doi.org/10.3390/aerospace9030136, 2022.

Zent, A. P., Hecht, M. H., Hudson, T. L., Wood, S. E., and Chevrier, V. F.: A revised calibration function and results for the Phoenix mission TECP relative humidity sensor: Phoenix Humidity Results, J. Geophys. Res. Planets, 121, 626–651, https://doi.org/10.1002/2015JE004933, 2016.